Article

Not peer-reviewed version

Unraveling the Photoelectrochemical Properties of $Bi_{12}NiO_{19}$: A Novel p-Type Photocatalyst for Efficient Visible-Light Driven Dye Degradation

Ahmed Malek Djaballah *, Radia Bagtache *, Mohamed Trari

Posted Date: 21 July 2025

doi: 10.20944/preprints202507.1568.v1

Keywords: selenite $Bi_{12}NiO_{19}$; p-type semiconductor; photoelectrochemistry; visible-light; photocatalysis; methyl violet degradation; sol gel synthesis

 doi:10.20944/preprints202507.1568.v1

Article

Unraveling the Photoelectrochemical Properties of $Bi_{12}NiO_{19}$: A Novel p-Type Photocatalyst for Efficient Visible-Light-Driven Dye Degradation

Ahmed Malek Djaballah [1,*], Radia Bagtache [2,*] and Mohamed Trari [3]

[1] Laboratory of Electrochemistry-Corrosion, Metallurgy and Inorganic Chemistry, Faculty of Chemistry, (USTHB), BP 32, 16111, Algiers, Algeria

[2] Institute of Physical Chemistry, Polish Academy of Sciences, Kasprzaka 44/52, 01-224 Warsaw, Poland

[3] Laboratory of Storage and Valorisation of Renewable Energies, Faculty of Chemistry, (USTHB), BP 32, 16111, Algiers, Algeria

* Correspondence: amdjaballah@ichf.edu.pl (A.M.D.); bagtacheradia@yahoo.fr (R.B.)

Abstract

$Bi_{12}NiO_{19}$ was synthesized through a sol–gel technique employing citrate as a complexing agent. Structural confirmation via X-ray diffraction revealed a pure phase with an average crystallite size of approximately 32 nm. Optical analysis indicated a direct band gap of 2.38 eV, linked to Ni^{2+} ($3d^6$) transitions, suggesting strong absorption in the visible spectrum. The material exhibited p-type conductivity and favorable charge transport characteristics, as evidenced by photoelectrochemical measurements. Mott–Schottky plots in 0.1 M Na_2SO_4 electrolyte identified a flat band potential of 0.67 V vs. SCE, with valence and conduction bands located at 0.87 V and –1.51 V vs. SCE, respectively, corresponding to O^{2-}:2p and Bi^{3+}:6p contributions. The photocatalytic activity of $Bi_{12}NiO_{19}$ was assessed for the degradation of Methyl Violet (MV) under visible-light exposure. A removal efficiency of 60% was achieved after 4 hours, primarily due to the formation of superoxide radicals ($O_2^{\bullet -}$). Kinetic studies followed a second-order reaction model with a photocatalytic half-life of 30 minutes. These results demonstrate the promise of $Bi_{12}NiO_{19}$ as a novel p-type photocatalyst for environmental remediation under visible light.

Keywords: selenite $Bi_{12}NiO_{19}$; p-type semiconductor; Photoelectrochemistry; Visible-Light Photocatalysis; Methyl Violet Degradation; Sol Gel Synthesis

1. Introduction

The textile and dyeing industries consume vast amounts of water and release considerable quantities of untreated dyes into aquatic ecosystems. It is estimated that nearly 20% of global dye production is discharged into the environment without adequate treatment (Osterloh et al., 2018; Walter et al., 2018; Kudo et al., 2011). The persistence and chemical stability of many modern dyes—especially those used in growing textile applications make them resistant to conventional degradation methods. Consequently, textile wastewater poses significant environmental and health hazards, necessitating advanced and targeted treatment technologies (Maeda et al., 2013; Bagtache et al., 2014; Bulte et al., 2004).

Among synthetic dyes, azo compounds represent over 60% of those used in industrial applications (Bagtache et al., 2019). These molecules exhibit high stability and low biodegradability due to their conjugated double bonds and mesomeric structures, and many are classified as toxic or carcinogenic (Helaili et al., 2010; Sabri et al., 2020). To address the ecological risks associated with dye-contaminated effluents, several treatment approaches have been proposed, including biological processes (Djaballah et al., 2022), adsorption (Bagtache et al., 2021), sonolysis (Sahmi et al., 2024), and photocatalysis.

 doi:10.20944/preprints202507.1568.v1

Photocatalysis has emerged as a particularly effective method for the degradation of a broad range of organic pollutants, including dyes (Bagtache et al., 2020), pesticides (Bagtache et al., 2022), pharmaceutical residues (Banat et al., 1996), and antibiotics (Kaci et al., 2021). Various semiconductor materials have been employed for this purpose, with metal oxides such as bismuth-based compounds gaining attention due to their cost-effectiveness, ease of synthesis, chemical stability, and environmental compatibility (Ben Aziza et al., 2021; Baaloudj et al., 2021; Vijay Kumar et al., 2018).

In this context, the present work focuses on the synthesis and detailed physical, chemical, and photoelectrochemical characterization of the selenite phase $Bi_{12}NiO_{19}$. The material was prepared via a sol–gel route and applied for the first time to the visible-light-induced degradation of Methyl Violet (MV), a model pollutant representative of synthetic dyes.

2. Experimental

2.1. Material and Methods

2.1.1. Synthesis of $Bi_{12}NiO_{19}$

One widely used synthesis approach for complex oxides involves the decomposition of metal nitrates. In this study, $Bi_{12}NiO_{19}$ was synthesized via a citrate-assisted sol–gel route. High-purity bismuth nitrate [Bi $(NO_3)_3 \cdot 9H_2O$] and nickel nitrate [Ni $(NO_3)_2 \cdot 6H_2O$] (≥99%) were dissolved in distilled water. To the resulting clear solution, 5% excess citric acid was added under continuous stirring, followed by gentle heating until the formation of a viscous gel. This gel was subsequently heated at 350 °C for 2 hours on a hot plate to promote the removal of nitrogen oxides (NO_x) fumes.

The obtained precursor was further calcined in air at 400 °C for 3 hours, then ground into fine powder. The powder underwent a first calcination step at 600 °C for 3 hours, followed by a second calcination at 800 °C for 3 hours. The final product was air-quenched to facilitate the incorporation of bismuth into the lattice and to obtain the crystalline $Bi_{12}NiO_{19}$ phase.

2.2. Characterisation

The crystal structure of the synthesized $Bi_{12}NiO_{19}$ powder was elucidated using X-ray diffraction (XRD) performed on an X'Pert Pro diffractometer with Cu Kα radiation (λ = 1.54 Å). The morphology of the powder was examined by scanning electron microscopy (SEM) using a Schottky field emission microscope (FESEM; JSM-7610F Plus, JEOL). Optical properties were investigated through diffuse reflectance measurements recorded on a Jasco 650 UV/Vis spectrophotometer within the 190–900 nm wavelength range. Photoelectrochemical characterization was carried out in a conventional three-electrode cell filled with 0.1 M Na_2SO_4 electrolyte solution. A saturated calomel electrode (SCE, $Hg/Hg_2Cl_2/Cl^-$) served as the reference electrode, while a platinum gauze functioned as the counter electrode. The working electrode consisted of an annealed $Bi_{12}NiO_{19}$ pellet (1.32 cm^2) electrically connected via a copper wire to its back face and sealed inside a Teflon tube with hardening araldite to ensure proper insulation. Current–potential (J–E) characteristics were recorded at a scan rate of 10 $mV \cdot s^{-}$ The flat band potential (E_fb), critical for understanding photocatalytic activity, was determined from Mott–Schottky plots of the inverse square capacitance (C^{-2}) versus applied potential at a frequency of 10 kHz to suppress the influence of the electrical double layer. Additionally, electrochemical impedance spectroscopy (EIS) measurements were performed over a frequency range from 10^{-2} to 10^5 Hz at the stabilized open circuit potential to further probe the interfacial charge transfer processes.

2.2.1. Point of Zero Charge (pH_{PZC})

The zero charge point (pHpzc) of $Bi_{12}NiO_{19}$ was: 25 mg of $Bi_{12}NiO_{19}$ was mixed with 25 mL of $NaNO_3$ solutions (0.1 M), the pH was adjusted in the range (2 – 12) by the addition of HCl or NaOH (0.1 N). The solutions were kept stirring (48 h) and the final pH was measured; the curves were plotted and pHpzc corresponds to the intersection point of the curves ($pH_{final} = pH_{initial}$).

 doi:10.20944/preprints202507.1568.v1

2.2.2. Photo Degradation

The photocatalytic performance of $Bi_{12}NiO_{19}$ was assessed through the visible-light-driven oxidation of Methyl Violet (MV). Experiments were conducted in a double-walled Pyrex photoreactor designed to maintain the reaction temperature at 25 ± 1 °C, minimizing thermal effects. A suspension of 10 mg of $Bi_{12}NiO_{19}$ was magnetically stirred at 400 rpm in 10 mL of MV solution (10 ppm) in the dark for 24 hours to achieve adsorption–desorption equilibrium. Subsequently, the solution was irradiated with a 14 W LED lamp emitting visible light at an intensity of 23 $mW \cdot cm^{-2}$, positioned 5 cm from the reaction mixture. The pH of the solution was kept at its natural value (~7) throughout the experiment. The concentration of MV was periodically monitored using UV-Vis spectrophotometry (Jasco 650) by measuring absorbance at 582 nm (λ_max). Concentration values were accurately determined via linear interpolation from a pre-established calibration curve. For comparison and control, photolysis tests without the catalyst were also performed under identical conditions.

3. Results and Discussion

3.1.1. Characterization of $Bi_{12}NiO_{19}$

3.1.1. Phase Identification

To identify the selenite phase $Bi_{12}NiO_{19}$, XRD analysis was used (Figure 1). All peaks belong to single phase $Bi_{12}NiO_{19}$ according to the JCPDS Card N°: 43-0448 (SG: I 23) (Brahimi et al. 2021). The least square method was used to refine the lattice parameters (a= 10.2406 Å). The good crystallization is evidenced from the narrow peak. The crystallite size calculated from.

The average dimension of the crystallites was calculated from the Williamson Hall (W-H) relation (Equ. 1), which shows the contribution of the size broadening (kλ/d) and strain broadening (η sinθ) (Nithya et al. 2020; Hosseinzadeh et al. 2022):

$$\beta \cos(\theta) = (k\lambda/D) + (\eta \sin\theta) \quad (1)$$

The β broadening is a function of instrumental parameters, induced defects and strain, in the crystal structure (Inset Figure 1). A size of 32.38 nm was deduced from the extrapolation of the line "β cosθ" with the y-axis

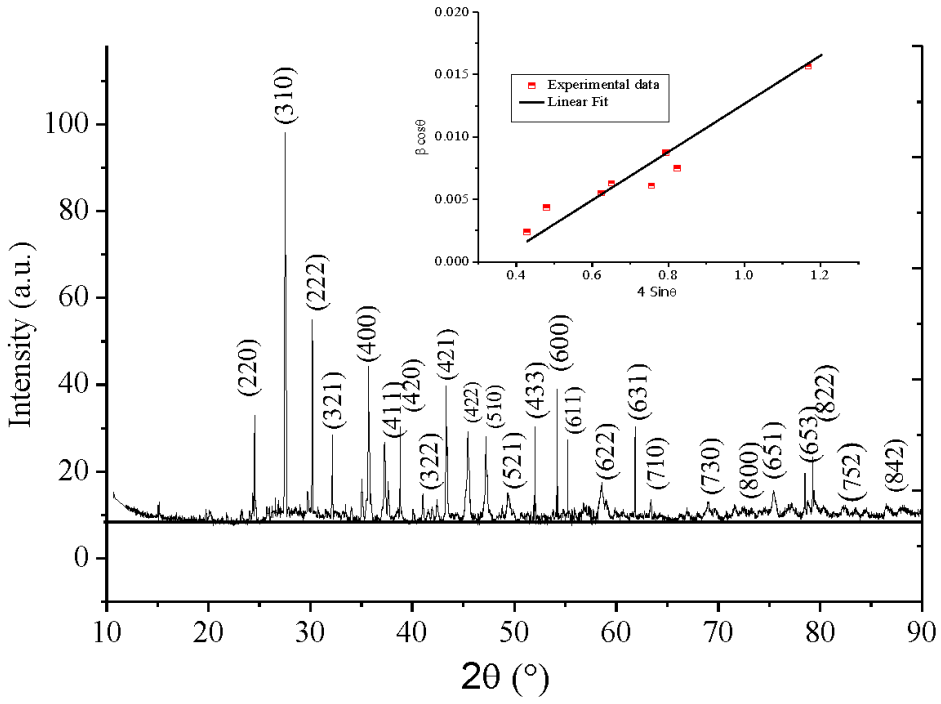

 doi:10.20944/preprints202507.1568.v1

Figure 1. XRD pattern of the selenite $Bi_{12}NiO_{19}$ prepared by citrate route. Inset crystallite size calculation by WH plot.

3.1.2. Optical Study

Photoactivity is primarily conditioned by the band gap (E_g) value (Figure 2). The optical characteristics of $Bi_{12}NiO_{19}$ were determined by UV-Vis diffuse reflectance by studying the dependence of the absorption coefficient ($\alpha\lambda$) on the photon energy ($h\nu$) using the relation:

(Thi Mai Tho et al. 2020 ; Hsieh et al. 2013):

$$F(R_\infty) = \alpha\lambda = (1 - R_\infty)^2 / 2\,R_\infty \quad (2)$$

This technique is based on the value of the absorption coefficient ($\alpha\lambda$, cm^{-1}) which is a function of λ, $R\infty$ is obtained from the diffuse refectance data (R%), taken from the diffuse reflectance spectrum. The optical gap (E_g) is deduced by extrapolation of the line with the abscissa axis in accordance with the relation (Meng et al. 2015):

$$(\alpha\lambda h\nu)^{1/n} = K \times (h\nu - E_g) \quad (3)$$

where K is an intrinsic factor while the transition nature is indicated by the ***n*** value, equal to 0.5 and 2 respectively for direct and indirect optical transition. The line (Figure 2 a, Inset) shows that the selenite $Bi_{12}NiO_{19}$ with a yellow colour has a high absorption in the UV-Visible range, with two bands at 400 and 715 nm where the fraction of the light irradiance is converted into electrical and/or chemical energy (Zhoua et al. 2021). An additional direct transition at 2.38 eV (***n*** = 2) is also observed (Figure 2b). The narrow gap makes the selenite an attractive photocatalyst for water treatment or photovoltaic conversion (Pei et al. 2016, Rajamoorthy et al. 2021).

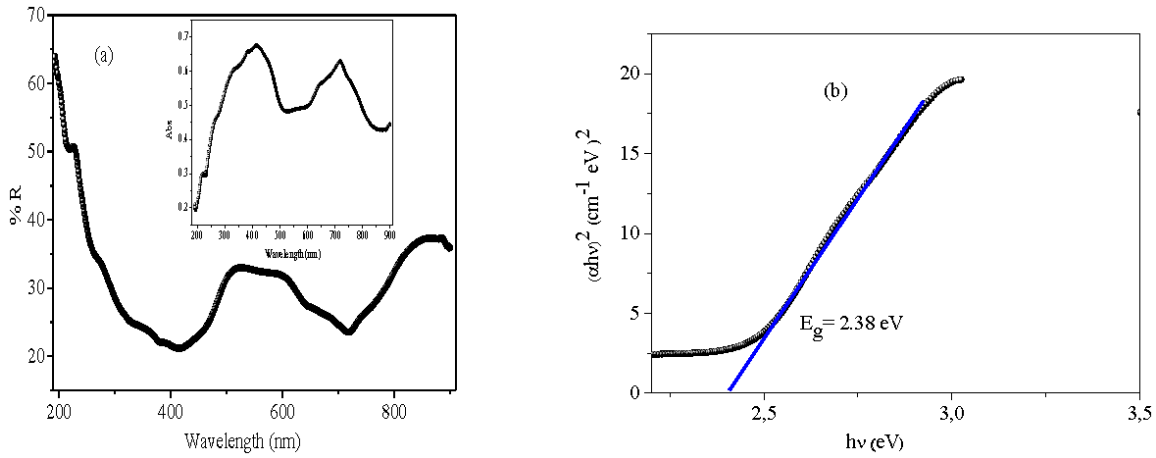

Figure 2. (a) UV–Vis diffuse reflectance spectrum of $Bi_{12}NiO_{19}$. Inset: the absorbance UV and (b) direct optical transition.

3.1.3. Morphology

Scanning Electron Microscopy (SEM) was used to capture the morphology of the $Bi_{12}NiO_{19}$ powder. The SEM images show small agglomeration can be seen due to the ultrafine nature of the sample, prepared hydrothermally (Figure 3a) with a non-uniform distribution of crystals of different shapes. The existence of the constituting elements (Ni, Bi, and O) of the selenite was confirmed by the EDX spectrum (Figure 3b), with a composition close to the nominal one.

 doi:10.20944/preprints202507.1568.v1

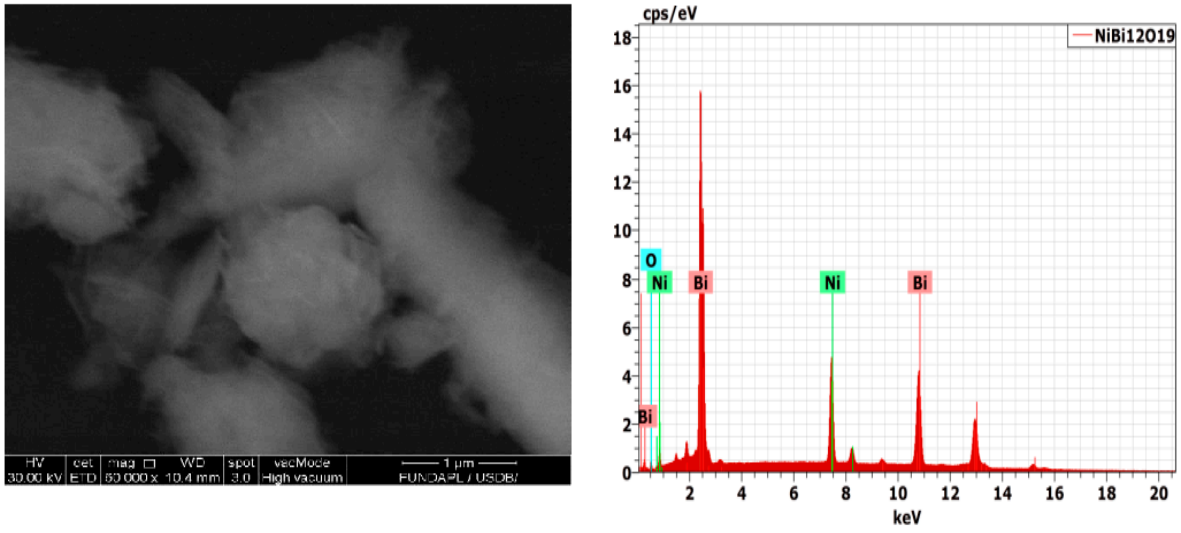

Figure 3. SEM image and EDX analysis of $Bi_{12}NiO_{19}$ synthetized by citrate route.

3.1.4. Electrochemical Properties

Cyclic voltammetry of $Bi_{12}NiO_{19}$ is plotted to examine its behaviour and stability in the working solution (Na_2SO_4). Figure 4 presents the J(E) characteristics in the dark. The current averages at ~ 0.2 mA cm^2 and decreases below -0.9 V without a diffusion plateau, due to the evolution of H_2; the band at ~ -0.5 V corresponds to the reduction of oxygen

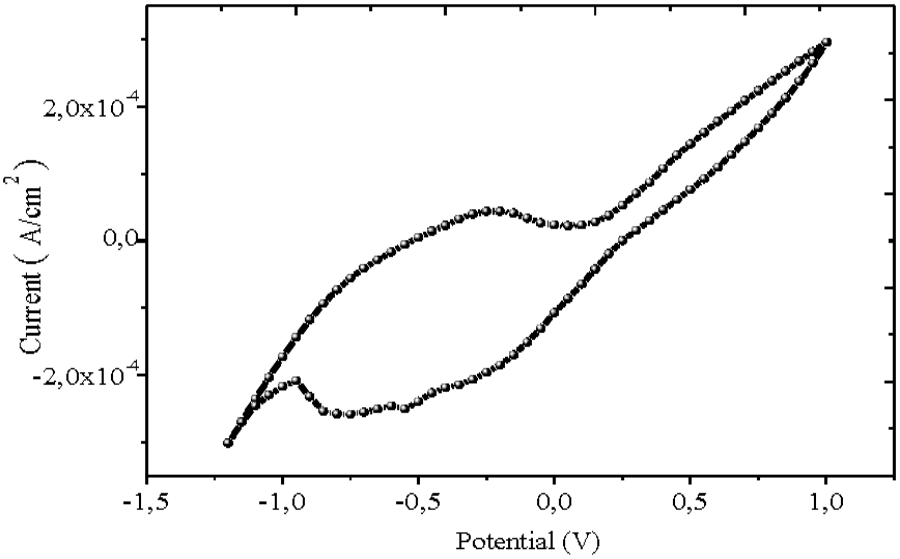

Figure 4. The cyclic voltammetry J (E) of $Bi_{12}NiO_{19}$ plotted in air saturated Na_2SO_4 (0.1 M) electrolyte.

Selenite is used in photocatalysis and electrochemistry is required to delimit the electroactivity domain and localize the electronic bands in the potential scale. Cyclic voltammetry of $Bi_{12}NiO_{19}$ is undertaken to elucidate the behaviour and its stability in the working solution (Na_2SO_4). J(E) characteristics plotted in the dark and under visible light are shown in Figure 4. The current density is around 0.2 mA cm^2 and decreases below -0.9 V without reaching a diffusion plateau, due to the evolution of H_2. The band at about -0.5 V corresponds to the reduction of oxygen ($2\ H_2O + O_2 + 2\ e^- \rightarrow H_2O_2 + 2\ OH^-$) (Ma et al. 2019). To corroborate the *p* type nature of the Selenite, we have undertaken a chrono-amperometry under chopped visible light (Figure 5); the electrode was polarized at -0.25 V, a potential more cathodic than the potential E_{fb}. The increased cathodic current brings an unambiguous confirmation of *p*-type behaviour. The flat band potential (E_{fb}) is essential for

 doi:10.20944/preprints202507.1568.v1

predicting the photocatalytic reactions (Pant et al. 2013) and is reliably determined from the capacitance measurement et high frequency (10 kHz) using the relation (Pant et al. 2019):

$$C^{-2} = \pm (2/e\,\varepsilon_o\,\varepsilon\,N_{D/A})\,\{V - V_{fb} - kT/e\} \quad (4)$$

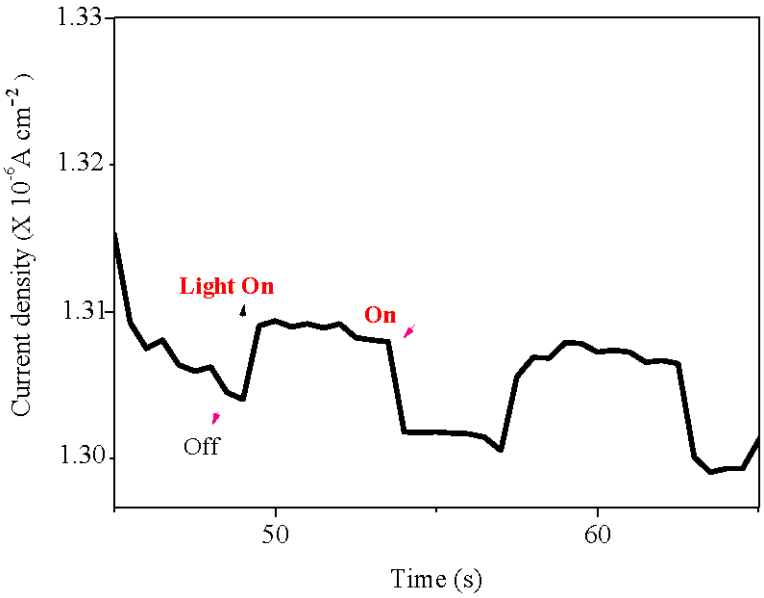

Figure 5. Chrono-amperometry of $Bi_{12}NiO_{19}$ under chopped visible light in Na_2SO_4 solution (0.1 M). The electrode was biased at a potential of -0.25 V.

The *p*-type conduction is corroborated by the negative slope with holes as dominant charge carriers. A potential E_{fb} of 0.67 V was determined by extrapolating the line to infinite capacity (C^{-2} = 0) (Figure 6). The energy/potential of the valence band (E_{VB}: 5.62 eV/0.87 V_{SCE}) indicates that VB is formed by the orbital O^{2-}: *2p* while the conduction band (E_{CB} 3.24 eV/- 1.51 V_{SCE}) is made up of Bi^{3+}: *6s* orbital. The potential of the bands CB and VB are given by (Li et al. 2017):

$$E_{VB} = 4.75 + |e| \times E_{fb} + 0.059\,(pH - pzc) + E_a \quad (5)$$

$$E_{CB} = E_{VB} - E_g \quad (6)$$

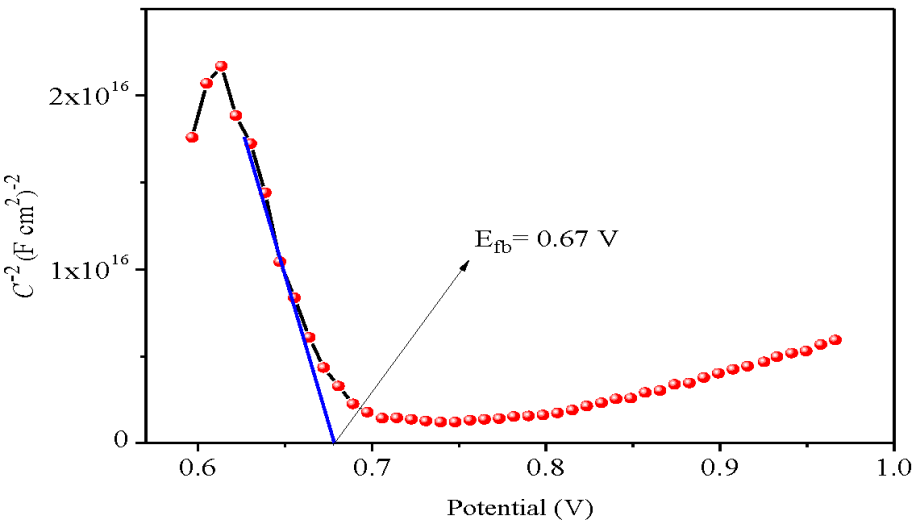

Figure 6. The capacitance-potential (C^{-2} – E) characteristic of Bi12NiO19 plotted in Na_2SO_4 electrolyte at a frequency of 10 kHz.

 doi:10.20944/preprints202507.1568.v1

The EIS analysis was used to elucidate the electron transfer across the $Bi_{12}NiO_{19}$/liquid interface over a large frequency range in Na_2SO_4 solution at stabilized free potential (OCP = 0.11 V). The complex diagram i.e. the imaginary part ($-Z_{imag}$) against the real part (Z_{real}) both in the obscurity and under visible light (Figure 7). The centres of the semicircles are not positioned on the real axis and this implies a deviation from a purely capacitive behaviour with existence of a constant phase element (CPE) (Djellal et al. 2009):

$$Z = Q\,(jW)^{-m} \tag{7}$$

the homogeneity factor m, between 0 and 1, is related to the phase angle φ {= (mπ/2)} and Q a constant independent of the frequency. EIS correlates the morphology to the interfacial mechanism and quantifies the contributions of the bulk, grain boundaries and ion diffusion as well as the microstructure of the compound to the transport properties (Su et al. 2018).

The semi-circle is associated to the charge transfer resistance (R_1 = 674 Ω cm²) whose diameter falls down to 485 Ω cm² under visible irradiation, corroborating the semi conductivity of $Bi_{12}NiO_{19}$, The offset near the origin is attributed to the electrolytic solution R_s = 759 Ω cm² (Table 1). The data are fitted to an equivalent electrical circuit by the Zview software (Figure 7, Inset). The formation of the double layer due to the adsorption of ions generates a potential gradient, coming mainly from H^+ and OH^- ions; the quantity ΔpH = 0.059 (pH − pzc) at 25 °C can be neglected. The point of zero charge (pHpzc = 9.59) is determined from the drift method (Figure 8).

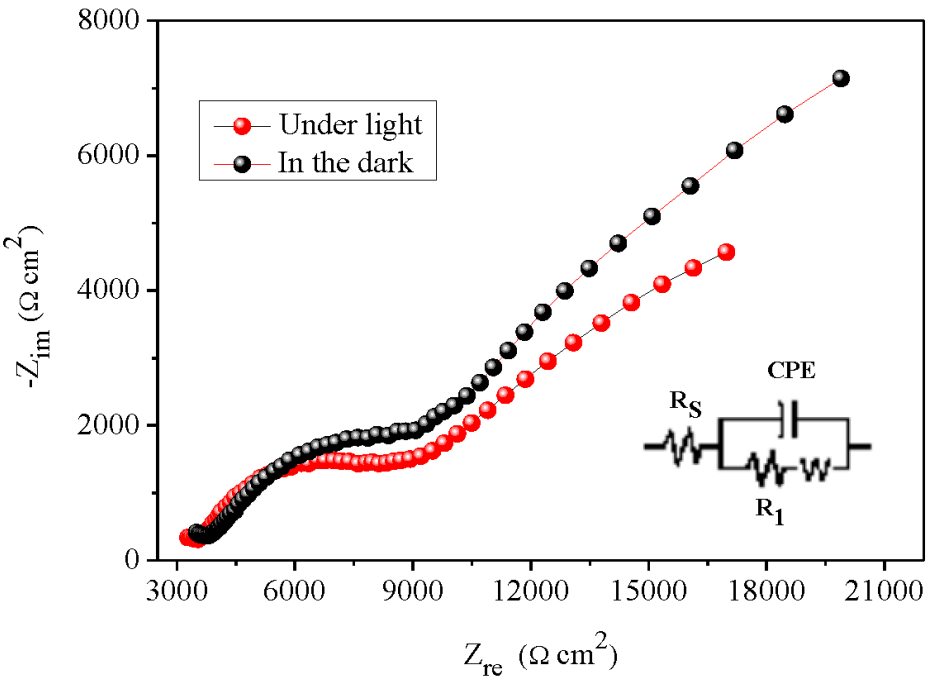

Figure 7. The EIS analysis of $Bi_{12}NiO_{19}$ in the dark and under visible illumination in Na_2SO_4 solution (0.1 M).

Table 1. The electrical parameters of the junction $Bi_{12}NiO_{19}$ /electrolyte Na_2SO_4 solution 0.1 M determined by Zview software.

$Bi_{12}NiO_{19}$	R_s (Ω cm^2)	CPE (F sec $^{1/n}$)	*n*	R_1 (Ω cm^2)	Ws (F sec $^{1/2}$)
In dark	983	3.68×10^{-6}	0.5	674	3.19×10^{-4}
Under Light	759	4.18×10^{-9}	0.5	486	3.07×10^{-4}

 doi:10.20944/preprints202507.1568.v1

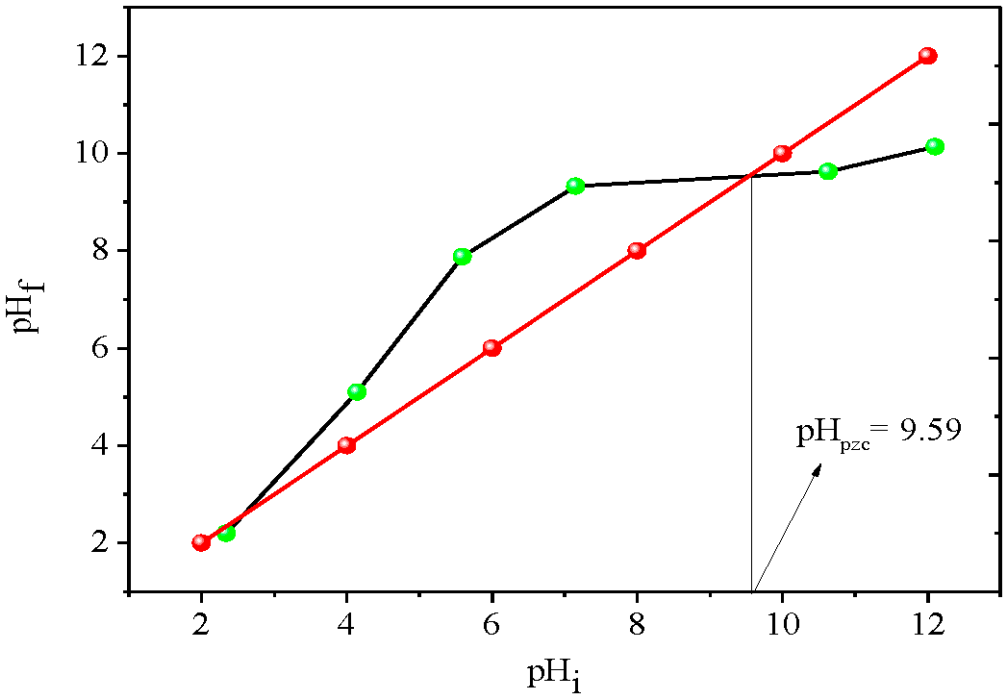

Figure 8. Determination of the point of zero charge (pH_{pzc}) of $Bi_{12}NiO_{19}$.

3.2. Photoactivity

Currently, the removal of pollutants from wastewater is a hot topic and photocatalysis is one of our research themes. $Bi_{12}NiO_{19}$ was chosen because of its band gap, allowing it to generate $O_2^{\bullet-}$ radicals (Zhang et al. 2017). However, $^{\bullet}OH$ species cannot be formed because the BV potential (0.87 V) is not anodic enough to oxidize water to $^{\bullet}OH$ capable of oxidizing the MV dye to mineral end products. An initial concentration of MV (10 mg/L), commonly encountered in effluents, was used and the reaction mechanism on the surface of $Bi_{12}NiO_{19}$ was proposed (Zhang et al. 2016):

$$Bi_{12}NiO_{19} + h\nu \rightarrow e^-_{CB} + h^+_{VB} \quad (8)$$

$$h^+_{VB} + H_2O \rightarrow {}^{\bullet}OH + H^+ \quad (9)$$

$$e^-_{CB} + O_2 \rightarrow O_2^{\bullet-} \quad (10)$$

$$MV + {}^{\bullet}OH \,/\, O_2^{\bullet-} \rightarrow \text{Degradation products} \quad (11)$$

Adsorption, the first step in photocatalysis, depends on the surface charge of $Bi_{12}NiO_{19}$, governed by pHpzc. A pseudo-second-order kinetic has been successfully tested for photo-oxidation (Chang et al. 2018):

$$1/C_t = k\,t + 1/C_o \quad (12)$$

where t is the reaction time (min) and $\boldsymbol{k}$ the degradation rate constant (min^{-1}). It is worthwhile to mention that 13 % of MV are removed by photolysis (without catalyst) (Figure 9b) while an elimination percentage of 60% was reached after 240 min under visible irradiation (Figure 9a). The rate constant (k) is calculated from the slope of the line $1/C_t$ vs. t (Figure 10); giving a photocatalytic half-life of 30 min. The H_2 production onto the selenite under visible light irradiation will be the objective of our next paper.

where $\boldsymbol{t}$ is the reaction time (min) and $\boldsymbol{k}$ the rate constant (min^{-1}). It is worth noting that 13% of MV was eliminated by photolysis (Figure 9b). In contrast, 60% reduction was reached after 4 h under visible light illumination (Figure 9a). The constant $\boldsymbol{k}$ is deduced from the slope of the line $1/C_t$ vs. $\boldsymbol{t}$

 doi:10.20944/preprints202507.1568.v1

(Figure 10); a photocatalytic half-life of 30 min was deduced. More interestingly, we noticed that the H_2 evolution occurs simultaneously, due the conduction band (-1.5 V) cathodic than the H_2 level (~ -0.8 V) on the selenite. Therefore, the H_2 production on selenite under visible light irradiation will be the focus of our next article.

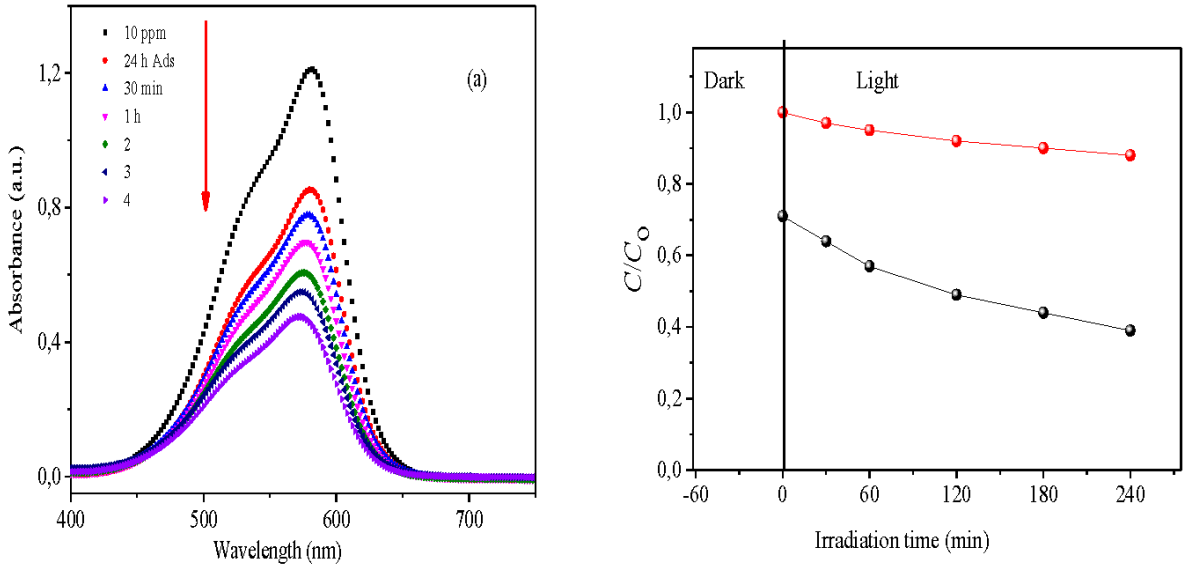

Figure 9. (a) Photo-degradation and (b) comparison between photolysis and photocatalysis of the MV degradation on $Bi_{12}NiO_{19}$ under visible light.

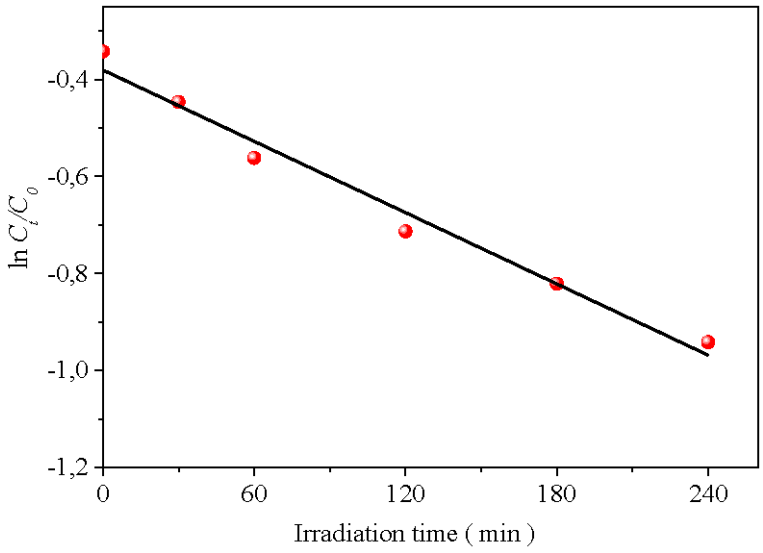

Figure 10. The pseudo-first-order kinetic of the MV degradation on $NiBi_{12}O_{19}$ under visible light.

4. Conclusion

In this study, $Bi_{12}NiO_{19}$ was successfully synthesized via a citrate-assisted sol–gel route, producing a well-crystallized cubic-phase p-type semiconductor with an average crystallite size of approximately 32 nm. Structural characterization confirmed the high purity and crystallinity of the material, while electron microscopy revealed particle agglomeration into heterogeneous grains. Optical investigations identified a direct band gap transition at around 2.38–2.87 eV, suitable for visible-light absorption. Electrochemical analyses established the semiconductor's p-type nature, with holes as majority carriers, and determined key parameters including a flat band potential of 0.67 V vs. SCE, alongside valence and conduction band edges formed mainly by O^{2-} (2p) and Bi^{3+} (6p)

 doi:10.20944/preprints202507.1568.v1

orbitals, respectively. The material exhibited excellent electrochemical stability in Na_2SO_4 solution, as evidenced by capacitance and chronoamperometric measurements.

Importantly, $Bi_{12}NiO_{19}$ demonstrated significant photocatalytic activity under visible light for the degradation of the synthetic dye Methyl Violet. A 60% degradation efficiency was achieved within 4 hours, driven primarily by reactive superoxide radicals ($O_2^{\bullet -}$). The photocatalytic reaction kinetics followed a pseudo-second-order model, with the high-energy Bi 6p orbitals playing a crucial role in facilitating effective charge transfer and dye oxidation. These findings not only highlight the potential of $Bi_{12}NiO_{19}$ as a cost-effective and environmentally friendly photocatalyst but also contribute valuable insights into the design of advanced p-type semiconductors for wastewater treatment applications.

Future work could explore doping strategies and composite formation to further enhance the visible-light absorption and charge separation efficiency of $Bi_{12}NiO_{19}$, aiming to optimize its photocatalytic performance for a broader range of organic pollutants. This study paves the way for the rational development of bismuth-based selenite oxides as promising candidates in sustainable environmental remediation technologies.

Data Availability Statement: The date presented in this manuscript is available with the corresponding author and can be provided on reasonable request.

Acknowledgments: This study was funded by the Faculty of Chemistry Grant N° B00L01UN160420190020 (USTHB; Algiers)

Conflicts of Interest: The authors declare that there is no known competing interests or personal relationships that could have appeared to influence the research work reported in this manuscript.

References

Al-Gheethi, A. A., & S. H. Z. (2018). "Removal of Methylene Blue Dye from Aqueous Solution Using an Eco-Friendly Bio-adsorbent: A Review." *Journal of Water Process Engineering*, 28, 143-153.

Bagtache, R., Abdmeziem, K., Rekhila, G., & Trari, M. (2019). "Synthesis, physical and electrochemical characterizations of organically templated cobalt-aluminophosphate. Application to oxygen evolution." *Journal of Materials Science: Materials in Electronics*, 30, 14928-14934.

Bagtache, R., Boudjedien, K., Djaballah, A. M., & Trari, M. (2022). "Photoelectrochemical characterization of Ag/CuCo2O4 prepared at low temperature: application to solar light oxidation of methyl orange." *International Journal of Environmental Science and Technology*, 19, 1-10.

Bagtache, R., Zahra, S., Abdi, A., & Trari, M. (2020). "Characterization of CuCo2O4 prepared by nitrate route: application to Ni2+ reduction under visible light." *Journal of Photo Chemistry and Photobiology A: Chemistry*, 400, 112728.

Banat, I. M., Nigam, P., Singh, D., & Marchant, R. (1996). "Microbial decolorization of textile-dye containing effluents: a review." *Bioresource Technology*, 58(3), 217-227.

Barakat, M., Badawi, M., & Trari, M. (2020). "Electrochemical characterization of CuCr2O4 photoanodes and their application in photoelectrochemical water splitting." *Journal of Energy Storage*, 30, 101459.

Ben Aziza, Meriem, et al. (2021). "The Influence of Different Stabilizers on Properties of Sol–Gel Spin-Coated Zinc Oxide Films." *Brazilian Journal of Physics*, 51(3), 722-730.

Boulhired, A., Halima, S., & Trari, M. (2023). "Green synthesis and characterization of ZnO/Ag3PO4 nanocomposite with enhanced photocatalytic activity." *Journal of Environmental Chemical Engineering*, 11(1), 108174.

Bousse, M. A., Mahmoud, A. K., & Trari, M. (2022). "Effect of doping on the photocatalytic activity of TiO2: A review." *Materials Science for Energy Technologies*, 8, 242-261.

Brahimi, B., Kenfoud, H., Benrighi, Y., & Baaloudj, O. (2021). "Structural and optical properties of Bi12NiO19 sillenite crystals: Application for the removal of Basic Blue 41 from wastewater." *Photochem*, 1(3), 319-329.

 doi:10.20944/preprints202507.1568.v1

Bulte, J.W., Kraitchman, D.L. (2004). "Iron oxide MR contrast agents for molecular and cellular imaging." *NMR in Biomedicine: An International Journal Devoted to the Development and Application of Magnetic Resonance In Vivo*, 17, 484-499.

Chang, C.J., Wang, C.W., Wei, Y.H., & Chen, C.Y. (2018). "Enhanced photocatalytic H2 production activity of Ag-doped Bi2WO6-graphene based photocatalysts." *Int. J. Hydrogen Energy*, 43, 11345-11354.

Djaballah, A. M., R. Bagtache, & M. Trari. (2022). "Physical and electrochemical properties of the spinel ZnBi2O4 prepared by citrate route: application towards photo degradation of methyl violet." *Journal of Materials Science: Materials in Electronics*, 33(23), 18410-18419.

Djemel, B., & M. Trari. (2023). "Photocatalytic properties of CuBi2O4 under visible light: A review." *Journal of Environmental Chemical Engineering*, 11(2), 107634.

Hosseinzadeh, G., Zinatloo-Ajabshir, S., & Yousefi, A. (2022). "Innovative synthesis of a novel ZnO/ZnBi2O4/graphene ternary heterojunction nanocomposite photocatalyst in the presence of tragacanth mucilage as natural surfactant." *Ceramics International*, 48, 6078-6086.

Hsieh, S.H., Lee, G.J., Davies, S.H., Masten, S.J., & Wu, J.J. (2013). "Synthesis of Cr2O3 and Pt doped RuO2/Bi2O3 Photocatalysts for Hydrogen Production from Water Splitting." *Am. J. Environ. Eng.*, 3, 115–120.

Kaci, M. M., et al. (2021). "Enhanced photocatalytic performance of CuAl2O4 nanoparticles spinel for dye degradation under visible light." *Research on Chemical Intermediates*, 47(9), 3785-3806.

Kudo, A. (2011). "Z-scheme photocatalyst systems for water splitting under visible light irradiation." *MRS Bulletin*, 36(1), 32-38.

Ma, Y., Qiu, F.L., Wei, T., Lin, F.F., Yan, L., Wu, H., Zhang, Y., Pei, L.Z., & Fan, C.G. (2019). "Facile Synthesis of Polyaniline/Bismuth Nickelate Nanorod Composites for Sensitive Tartaric Acid Detection." *Surf. Eng. Appl. Electrochem.*, 55, 335–341.

Maeda, K. (2013). "Z-scheme water splitting using two different semiconductor photocatalysts." *ACS Catalysis*, 3(7), 1486-1503.

Meng, Yuying, Deyang Chen, Yitao Sun, Dongling Jiao, Dechang Zeng, & Zhongwu Liu. (2015). *Applied Surface Science*, 324, 745-750.

N. Helaili, Y. Bessekhouad, A. Bouguelia, M. Trari. (2010). "p-Cu2O/n-ZnO heterojunction applied to visible light orange II degradation." *Solar Energy*, 84, 1187-1192.

Nithya, R., Ayyappan, S. (2020). "Novel exfoliated graphitic-C3N4 hybridised ZnBi2O4 (g-C3N4/ZnBi2O4) nanorods for catalytic reduction of 4-Nitrophenol and its antibacterial activity." *J. Photochem. Photobiol. A Chem.*, 398.

N.Thi Mai Tho, et al. (2018). "Mechanism of Visible-Light Photocatalytic Mineralization of Indigo Carmine Using ZnBi2O4-Bi2S3 Composites." *Chemistry Select*, 3, 9986–9994.

Pant, B., Pant, H.R., Barakat, N.A.M., Park, M., Jeon, K., Choi, Y., & Kim, H.Y. (2013). "Carbon nanofibers decorated with binary semiconductor (TiO2/ZnO) nanocomposites for the effective removal of organic pollutants and the enhancement of antibacterial activities." *Ceram. Int.*, 39, 7029–7035.

Pant, B., Ojha, G.P., Kim, H.Y., Park, M., & Park, S.J. (2019). "Fly-ash-incorporated electrospun zinc oxide nanofibers: Potential material for environmental remediation." *Environ. Pollut.*, 245, 163–172.

Pei, L.Z., Wei, T., Lin, F.F., Chen, X.J., Qiu, F.L., Ma, Y., Zhang, Y., Zhao, L., & Fan, C.G. (2020). "A Novel Polyaniline/Bismuth Nickelate Nanocomposite for Effective Photocatalytic Degradation of Dyes." *Chem. Eng. J.*, 399.

Pham, T.K., Ha, H.K., Kim, H.Y., Son, D.T., & Kim, S.K. (2020). "Synthesis of CeO2 nanoparticles using different methods: The structural and optical properties." *Powder Technology*, 368, 611-619.

Saad, A., Bouguelia, A., & Trari, M. (2023). "Copper oxide nanoparticles: synthesis, characterization, and photocatalytic properties under visible light." *Environmental Science and Pollution Research*.

Taha, A., Bouslama, R., & Trari, M. (2021). "Preparation and characterization of silver and copper nanoparticles for visible light photocatalysis." *Arabian Journal of Chemistry*, 14, 103279.

Tazout, M., Nasser, A., Merbouh, N., & Trari, M. (2022). "Recent advances in visible light photocatalytic activity of ZnO and its composite materials." *Journal of Environmental Chemical Engineering*, 10(2), 107049.

 doi:10.20944/preprints202507.1568.v1

Thi Mai Tho N., Nguyen Nha, Khanh D., Quoc Thang N., Yong-Ill Lee, Thi Kim Phuong Nguyen. "Novel reduced graphene oxide/ZnBi2O4 hybrid photocatalyst for visible light degradation of 2,4-dichlorophenoxyacetic acid", Environmental Science and Pollution Research, 2020

Trari, M., Bagtache, R., & Djaballah, A. M. (2020). "Recent advances in photocatalysis for water treatment." *Materials Today: Proceedings*, 27, 879-884.

Trari, M., Djemel, B., & Zahra, S. (2022). "Characterization and photocatalytic activity of synthesized ZnBi2O4 for dye degradation." *Journal of Environmental Chemical Engineering*, 10(1), 106998.

Trari, M., & Saad, A. (2019). "Photocatalytic performance of Cu2O nanoparticles for the degradation of organic pollutants." *Materials Today: Proceedings*, 16, 1673-1679.

Wang, S., Wang, P., & Zhang, L. (2020). "Nanostructured Photocatalysts for Environmental Remediation: Recent Advances and Future Challenges." *Journal of Hazardous Materials*, 382, 121195.

Zhang, Y., Wang, C., Wang, Y., & Wu, Z. (2016). "Fabrication of Bi2WO6/Ag3PO4 heterojunctions with enhanced photocatalytic activity." *RSC Advances*, 6, 11091-11097.

Zhang, Z., Zhao, Y., Zhang, Q., & Wang, Y. (2017). "Synthesis of Bi2S3/Bi2WO6 heterojunctions with enhanced photocatalytic activity under visible light." *Journal of Hazardous Materials*, 331, 99-107.

Zhou, H., Yang, H., & Zhai, Y. (2015). "Effects of temperature and humidity on the performance of TiO2 photocatalytic materials." *Journal of Photochemistry and Photobiology A: Chemistry*, 318, 64-70.

Zhoua, P.; Xiaoa, F.; Jia, L. Bi 12 NiO 19 micro-sheets grown on graphene oxide:Temperature-dependent facile synthesis and excellent electrochemical behavior forsupercapacitor electrode. J. Electroanal. Chem. 2021, 884, 115075.

Zou, G., Chen, W., Yang, Y., & Wang, J. (2019). "Novel preparation of nitrogen-doped TiO2 photocatalysts and their photocatalytic performance." *Journal of Materials Science*, 54(22), 14133-14142.